Homogenization of Primary Microsegregation

D. FAINSTEIN, G. F. BOLLING, AND H. BILONI

The homogenization kinetics of a segregated binary alloy have been studied using electron probe microanalysis after annealing for various times at several temperatures. The concentration and number of microsegregation nodes are quantitatively examined in detail and compared with the evolution of the whole solidification substructure revealed by X-ray images and metallography. The comparison leads to the conclusion that nodes are representative of all solidification substructure and can be taken as a characteristic. The combined study also shows that nodes dissolve in two stages, starting preferentially along cell walls and continuing later in a more uniform fashion. However, a single activation energy near that for bulk diffusion is obtained for the whole process, showing that the homogenization is a collective process and volume diffusion limited.

ONE feature of microsegregation substructures called nodes appears at the onset of constitutional supercooling and persists throughout freezing under more severe conditions.[1] These nodes are generally the regions of highest solute concentration, each localized within a few microns in cross-section and all distributed about a mean spacing of $\sim 50\ \mu$ for cubic metals (but nodes are not necessarily seen for the uncommon solutes with $k_0 > 1$). This pervasive feature of nodes as an element of substructures in general, provides a unique characteristic for all kinds of solidification substructures in the as-cast state. Furthermore, if it can be established that nodes are representative during dissolution, then any study of the homogenization of a solidified segregated alloy can reliably be based upon nodes.

Analyses of nodes and of a total substructure are both performed here on Al-0.34 pct Cu, a binary alloy that presents all the possible solidification substructure features through a cellular dendritic type. The results seem to be general for the evolution of the microsegregation pattern of any binary alloy following thermal homogenization.

Fine characteristics of nodes had to be taken into account in designing the experiments performed. As is well known,[2] nodes are generally prolate spheroids, exhibiting an approximately circular cross-section in a cut normal to the direction of growth. Any large enough sample of nodes will show the following features: a) variable sizes, both normal and parallel to the growth direction; b) variable size of cross-sections along the same node, both as a consequence of section and of morphology; c) solute concentrations that vary from node to node, independently of their size, and that vary in magnitude from within the range of solid solution, up to much higher values;[3] d) different concentration profiles even for such nodes whose measured maximum concentrations are the same.

As a result of the characteristics enumerated, dissolution must progress inhomogeneously throughout small volumes of an alloy sample and hence, the spatial distribution of the residual nodes changes with time in successive annealings. Different small areas in the same cross-section may show different morphological configurations of nodes, and even in an invariant section of any size, different spatial distributions will occur as the annealing time is increased. There are then, two different aspects which must be considered in studying the dissolution of nodes: 1) decrease in solute concentration as a function of the annealing time (concentration evolution), and 2) decrease in density (number of nodes per unit area) as a function of the annealing time (spatial evolution). Experiments can be designed statistically in order to meet with these multiple aspects of nodes and their evolution: 1) A large enough statistical sample is drawn out of the population of nodes, and microprobe analyses are done to determine concentration in the nodes of that sample. At the same time the dispersion of the population must be monitored in order to check the validity of the concentration evolution sampling. 2) In order to study the spatial evolution the sample must be chosen somewhat differently, as all the nodes in a fixed area of the analyzed surface, the size of the area being the same in all the analyses following isothermal anneals.

This simple statistical design has limitations that, although accountable, must be pointed out. The size of the area stated to be fixed in the initial as-cast specimens must be selected according to a null hypothesis.[4] As a consequence of both the spatial and the concentration evolutions, this null hypothesis can turn out to be false in a more advanced stage of annealing. Also, since the population varies inhomogeneously, the chosen sample can quite possibly have nodes which are not representative of the real population either in number or in concentrations. This last limitation, a consequence of real growth fluctuations, can be overcome by relying on an initial screening, such as rapid visual inspection of the surface, or by performing measurements of several samples, and averaging over the several statistics so obtained. One final limitation is more general or less benign in the sense that it is independent of the statistical design. The complete surface chosen might not be representative of the whole casting population in a particular stage. This must be discriminated by an inspection of photomicrographs both before and after particular anneals, which must show a consistent sequence; it cannot be bypassed by assem-

D. FAINSTEIN, currently on leave from CNEA, and G. F. BOLLING are with the Scientific Research Staff, Ford Motor Company, Dearborn, Mich. H. BILONI is with the Departmento de Metalurgia, Comisíon Nacional de Energía Atómica (CNEA), Buenos Aires, Argentina.

Manuscript submitted August 26, 1970.

bling some average, as just indicated for the simpler limitation.

I) EXPERIMENTAL PROCEDURES

a) General

An Al-0.34 wt pct Cu alloy was used in this investigation; for this composition the single phase region extends down below ~ 300°C. After small standard castings were poured, specimens were cut and polished first in the as-cast conditions. Thereafter specimens were polished after each thermal anneal prior to microprobe and metallographic analyses, since evolution was to be observed in the bulk.

A cellular dendritic pattern whose exact characteristics such as "dendrite arm spacing" will be shown to be relatively unimportant was obtained by casting, and two parallel cross-sections ~ 10 mm apart were found to be representative for any casting. Annealings were performed at four temperatures: 595°, 513°, 450°, and 400°C with maximum fluctuations registered as ±1.5°C. The shortest times for heating to annealing temperatures (~ 30 seconds) were obtained by using lead thermalized baths. The longest heat treatments were adequately performed in Chevenard furnaces.

b) Metallography

The detailed observation of each specimen's cut surface as a whole was an important complement to microanalysis, allowing comparison of the evolution (both in space and in concentration) undergone by the nodes with that of the total substructure. Detailed observation also proved to be the only means for observing the terminal evolution of the residual segregation of the alloy once the sensitivity of the microprobe was insufficient to resolve differences in composition. Metallographic observation is thus quite important and was carefully controlled; the specimens were electropolished for 20 min at 0°C under an applied voltage of 25 to 28 v, the electrolyte used being a mixture of 88 pct "butyl cello solve", 9.5 pct perchloric acid, and 2.5 pct glycerine.[5] Specimens were subsequently anodized using either a 10 pct H_2SO_4 aqueous solution at room temperature,[6] or a mixture of 60 pct of a 1 pct K_2CO_3 aqueous solution and 40 pct ethyl alcohol at 32° to 38°C.[5] In both cases the operating voltage was also 25 to 28 v. The periods of oxidation using the first solution varied from 20 sec to 1 min, and using the second about 8 min. The anodic film grown on the surface reveals the microstructure in great detail. The thickness of the film varies with orientation and composition, always giving a "color map" under oblique illumination, and even in bright field when the oxide is produced with the potassic solution.

c) Electron Microprobe Measurements

Microanalysis was performed at the operating voltage of 20 kv with a C.A.M.E.C.A. Ms 46 electron microprobe. $K\alpha_1$ radiation was monitored for copper and the solute content was measured both in nodes and in matrix. The instrument stability was well controlled, the operating conditions being checked at maximum intervals of 1 hr. Counting measurements were limited to 100 sec since longer time intervals might introduce errors due to contamination in the beam area.

Measurements were obtained with a 2 μ-diam beam (the smallest possible) in order to strive for the maximum concentration detectable in the nodes.[7] A 20 μ-beam was also used but no useful information was obtained, since the wide variety of node configurations made it impossible to establish any correlation between measurements with the 2 μ- and 20 μ-beams. Such estimates are consistent with elementary work previously done on similar alloys.[7]

The microprobe specimens were carefully polished to obtain the maximum smoothness required for the observation of nodes. A prolonged electropolishing must be avoided, since this can affect the cell walls of the cellular-dendritic structure and produce a microrelief which introduces a large absorption error in measurements, because the take-off angle is low (18 deg). The maximum surface distortions which were introduced were roughly estimated to have caused a reduction in the measured intensity by only 0.2 pct under the most unfavorable conditions allowed. This allowed value is less important than the lowest statistical errors; these occurred for the higher countings and were limited to 0.5 pct. The highest statistical excursions allowed in individual countings were 5 pct and, therefore, 5 pct was taken as the level of significance in deciding the size of the statistical sample. This statement of size (area) was determined by using the Tchebicheff inequality,[8] and the result was that the initial number of nodes should be $N \geq 80$. This size condition was further checked by actually performing separate measurements on two independent samples.[9]

d) Numerical Calculations of the Concentrations

The concentration data for the nodes were determined from the results obtained by microprobe measurements through computer calculations. With this objective a computer program was designed to allow the calculation of experimental concentrations (ratio of intensities measured in the specimen and in the standard, previously corrected for dead time of the counters and background noise) and their subsequent correction for secondary effects. These last corrections were done according to a ZAF scheme of corrections (Z: atomic number, A: absorption, F: fluorescence) in separate form,[10] and the results were introduced as a double entrance table experimental value/corrected value. The momenta of the distributions up to a high order were calculated in detail in an attempt to characterize the distributions completely; the results were statistically negative. The medians, kurtoses and asymmetries of the distributions were calculated for different statistical tests mentioned in the introduction as checks for validity; but apart from a statement that the statistics chosen could be validated, no results will be presented.[9]

Histograms of number of nodes as a function of copper concentration in intervals of 0.5 pct starting from 0.5 to 1 pct were made for each group of measurements; Fig. 1 is a collection of histograms showing the node concentration distributions after annealing at

400°C. It is typical of all the distributions obtained at other temperatures.

II RESULTS AND ANALYSIS OF THE EXPERIMENTS

Several statistics were available but the central one chosen for studying the concentration evolution of the nodes was the variation of the arithmetic mean $\bar{c}$ of the sample distribution after each isothermal anneal. Although this choice appears to be the most natural one since concentrations are the measured parameter, it must nevertheless be kept in mind that this statistic does not totally characterize the distributions obtained; the complete concentration information provided by the concentration histograms is always necessary for a satisfactory matching with the corresponding metallographic observations.

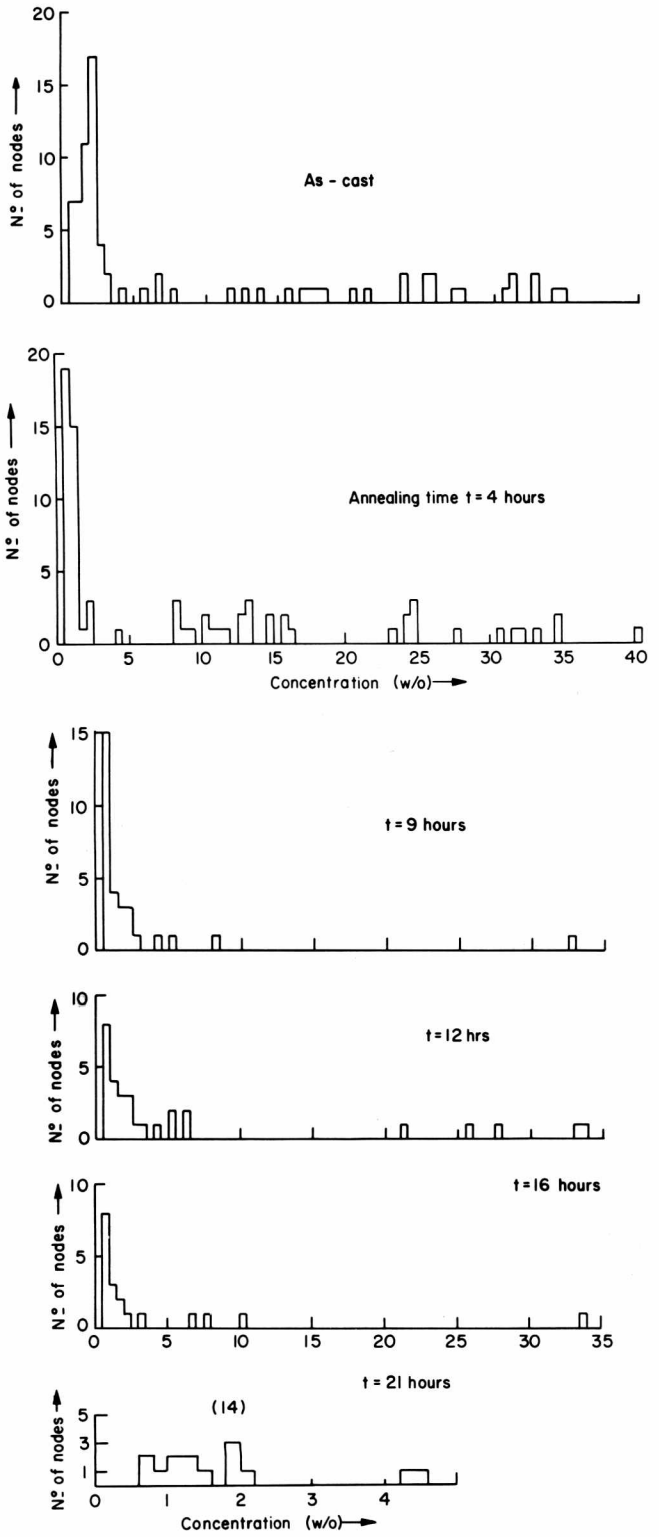

Fig. 1—Histograms showing the node concentration distributions after annealings at 400°C.

Results of concentration measurements in the matrix were not really helpful in determining a quantitative measure of the evolution. $\bar{c}$ (matrix) of course varies with time, as indeed could be deduced from the rapidly decreasing concentration difference between walls and matrix easily revealed by anodizing specimens for visual inspection during the initial stages of anneal. Another and more important observation also depends upon this type of visual inspection; during the later stages of anneal, while nodes containing second phase were visible, the cell walls never disappeared. In other words, the walls maintained a concentration difference from the matrix, no matter how slight.* In the microprobe analysis, individual measurements of such a distinction were beyond the sensitivity of the apparatus.

*This can even be seen by study of the black-and-white prints of Fig. 5; in color, the visual effect is more pronounced.

Other measurements for nodes, such as the values of the medians ($\hat{c}$ given in Table I) taken with $\bar{c}$, reveal the form of the concentration histograms and indicate a notable asymmetry in the node concentration distributions towards the low concentration values ($c \sim 2$ pct). This distribution phenomenon present in all stages of dissolution is to be expected because kinetics are slower for lower chemical gradients, so that higher concentration nodes (without extensive second phase) must evolve more rapidly thus leading to the asymmetry.

At 595°C the homogenization is so rapid that quantitative measurements were not feasible and qualitative metallographic observations were relied upon. After a 30 min anneal, homogenization of the whole specimen has progressed so considerably that the differences in composition are scarcely noticeable even with the help of the anodic film. A 15 min anneal showed a similar state, being practically indistinguishable from that of 30 min. After 5 min, the substructure could be recognized with broadened cell walls but no detectable nodes, that must have either been already dissolved or in very late stages of dissolution. Shorter annealing times were not useful, since the errors introduced in the determination of the time interval destroy the quantitative analysis. A short-time bound was thus the only critical information obtainable at this temperature.

Fig. 2 shows the time evolution of nodes at the other temperatures (400°, 450°, and 513°C). As immediately evident in the dissolution kinetics for 400°C and apparent for 450°C, $\bar{c}$ vs time shows turning points. The existence of these maxima and minima depends on a second phase in the nodes. Since the nodes are widely distributed in size as pointed out in the introduction, the proportion of second phase can vary in a nonuniform way and the concentration profiles, $\bar{c}$ vs t, must reflect this fact in an inhomogeneous variation and in the persistence of high concentration nodes until ad-

Table I. Annealing Times and Node Concentrations

Annealing Temperature, T = 400°C			Annealing Temperature, T = 450°C			Annealing Temperature, T = 513°C		
Total Annealing Time, hr	Mean $\bar{c}$, wt pct	Median $\hat{c}$, wt pct	Total Annealing Time, hr	Mean $\bar{c}$, wt pct	Median $\hat{c}$, wt pct	Total Annealing Time, min	Mean $\bar{c}$, wt pct	Median $\hat{c}$, wt pct
0	9.71	2.46	0	8.79	2.20	0	13.5	5.83
2	11.3	1.41	0.5	8.46	1.71	5	5.69	1.77
4	9.66	2.15	1	5.14	1.63	10	1.86	0.81
6	6.90	1.37	1.3	1.65	0.66	15	3.83	–
9	2.39	1.18	1.7	2.54	1.01	20	2.98	0.55
12	6.42	2.15	2	2.61	1.33	40;60	–	–
16	3.64	1.17	2.5	2.41	1.13	60;120	–	–
21	1.69	1.40	3	2.92	0.83	180;360	–	–
42;66	–	–	4	2.95	2.09			
			5	2.07	0.79	T = 595°C		
			8	2.91	1.36	5;15	–	–
			24;57	–	–	30	–	–

vanced dissolution stages. This latter persistence is immediately evident in the histograms, see Fig. 1. The inhomogeneous profile evolution arises because the lowest concentration nodes dissolve first and are removed from the population, resulting in an increase in $\bar{c}$. Since such behavior is stepwise, it can conceivably occur every time a concentration stage is passed, and so several inflections can be explained. At the higher annealing temperatures, inflections would not be easily observed during the initial stages because of the rapidity of the homogenization.

The ability to observe detail of this inhomogeneous population behavior is purely a consequence of the statistics employed. The means $\bar{c}$ obtained out of the node concentration distributions are only an absolute measurement of the mean concentration at each stage, in the sense that the spatial evolution of the nodes themselves are not taken into account. However, the mean density of nodes, $\bar{\rho}$, as a function of time, can also be taken into account, thereby providing a measure of the "overall dissolution kinetics" which accounts for both concentration and spatial changes. This is given by the product $\bar{c}\,\bar{\rho}$.

Values of $\bar{\rho}$ measured by simple counting are given in Figs. 3 and 4, showing $\bar{\rho}(t)$ on a semilogarithmic scale for all the kinetics studied. For the 400° and 450°C evolutions, two stages can be clearly distinguished. During stage I, log $\bar{\rho}$ decreases linearly, departing radically from this line at later times (stage II). Stage I extends approximately up to 12 hr, 20 min of annealing at 400°C and 2 hr, 30 min at 450°C. The departure of log $\bar{\rho}$ from an initial straight line coincides with an important morphological change; nodes with discernible second phase disappear near the transition zone and are not present in the far advanced dissolution after prolonged annealing. This can be deduced from the histograms of Fig. 1 (for 400°C), or seen directly in the micrographs of Fig. 5 (for 450°C to show generality), or seen indirectly in the X-ray images of Fig. 6 (for 513°C, again for generality).

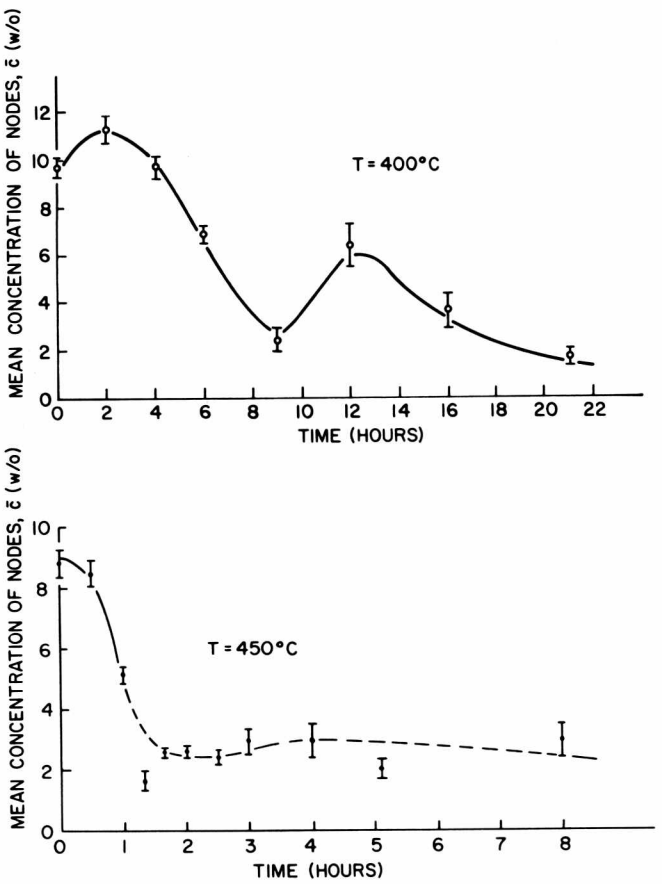

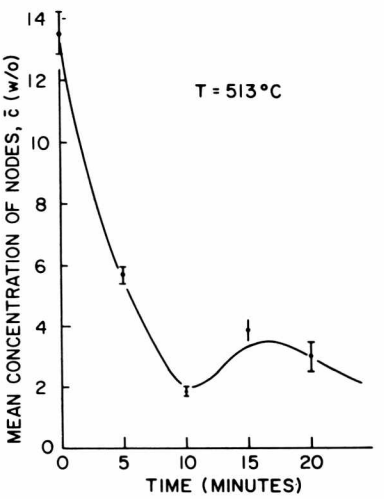

Fig. 2—Concentration evolution of nodes at various temperatures.

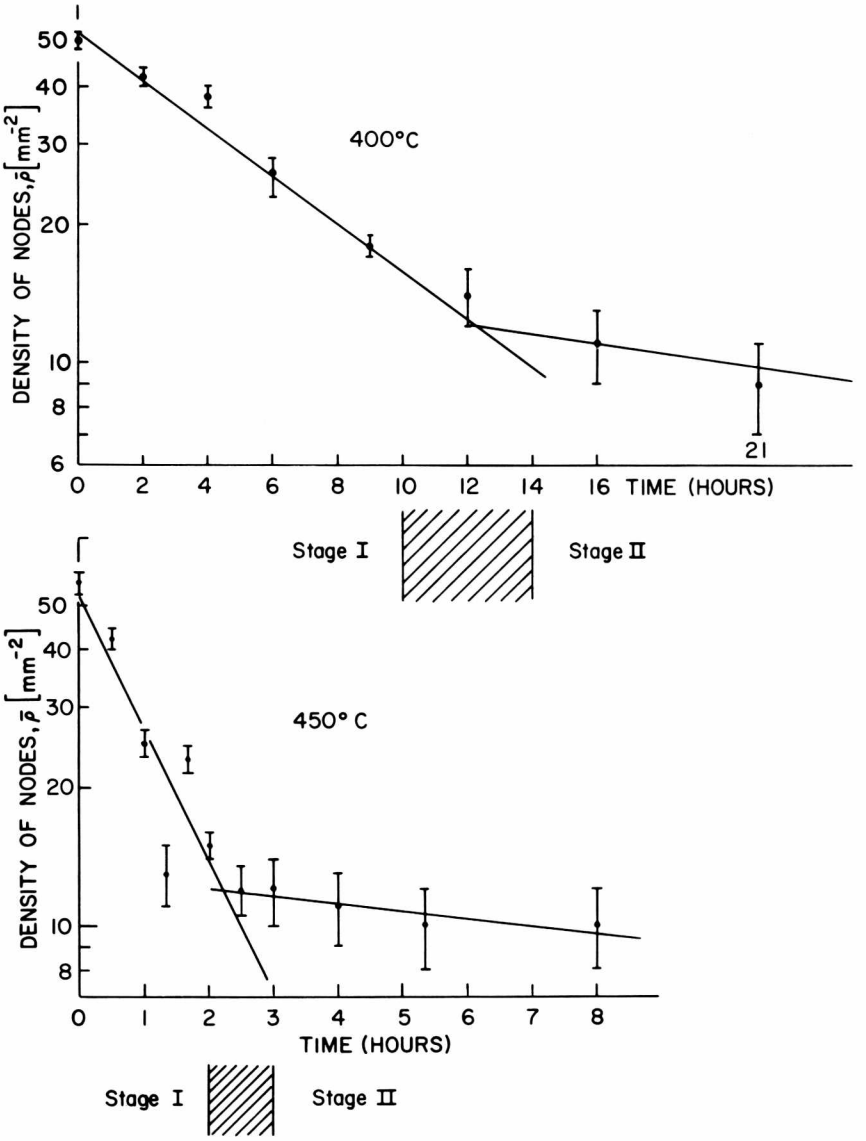

Fig. 3—Evolution of the density of nodes at 400° and 450° C.

The more rapid evolution which took place at 513°C did not allow the determination of node density after 20 min of treatment, since the pronounced decrease in concentration made microanalysis difficult. Annealings were continued nevertheless, and metallographic observations, when compared to those of the lower temperatures, allowed one to establish that a similar transition had indeed taken place at a time intermediate to 15 to 20 min consistent with Fig. 6. This conclusion is imposed in Fig. 4; a most probable evolution at 595°C is also based on a comparison with metallographic studies, giving the short-time bound already mentioned. In plotting Fig. 4 it was taken into account that for the slower kinetics, where the transition is clearly seen in Fig. 3, stage I extends between the same range of values for $\bar{\rho}$.

All the results for $\bar{\rho}$ and $\bar{c}$ vs time are presented in Fig. 7 as the product $\bar{\rho}\,\bar{c}$ on a normalized scale for the kinetics investigated. $\bar{\rho}\,\bar{c}$ decreases continuously as a function of time as was expected, since the spatial evolution as well as the concentration evolution have been explicitly included. $\bar{\rho}\,\bar{c}$ is also seen to decrease, within experimental error, to the same relative value at the transition times. Hence, $\bar{\rho}\,\bar{c}$ appears to be the proper

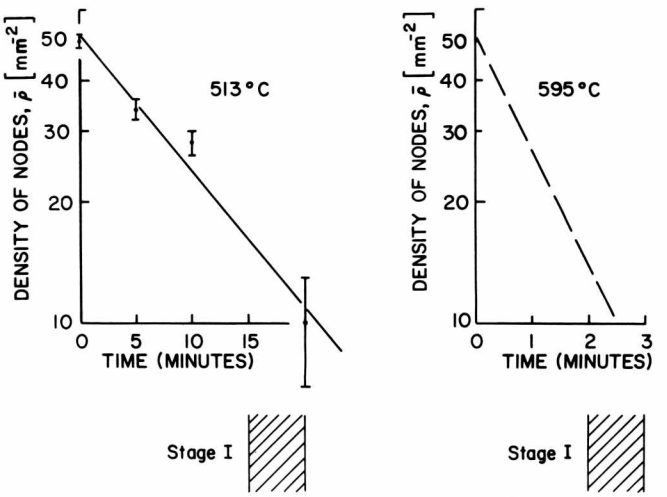

Fig. 4—Evolution of the density of nodes at 513° and 595° C.

statistic characterizing the kinetic processes studied.

The time elapsed for $\bar{\rho}\,\bar{c}$ to decrease to a given value at a given temperature must represent a characteristic time functionally involving the diffusion coefficient

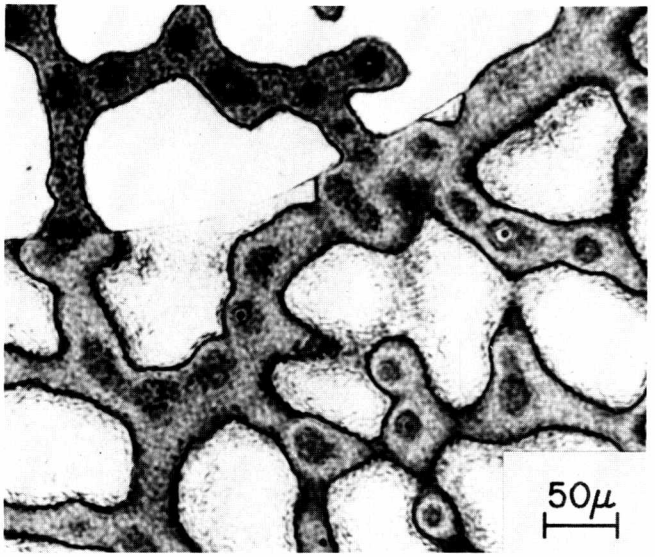

(a)

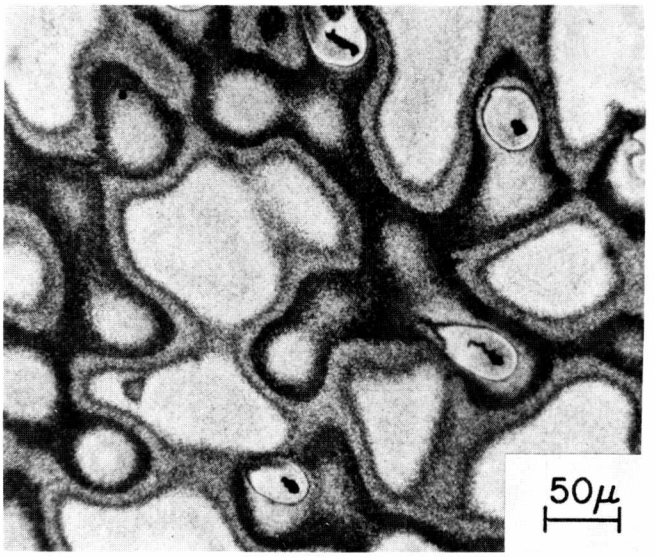

(b)

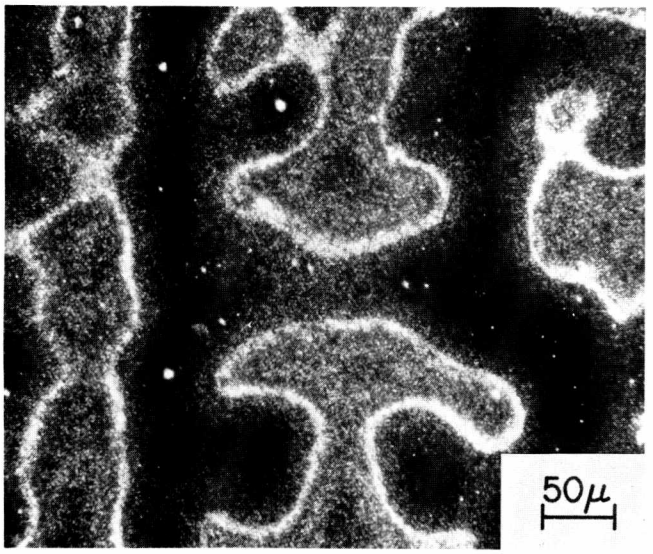

(c)

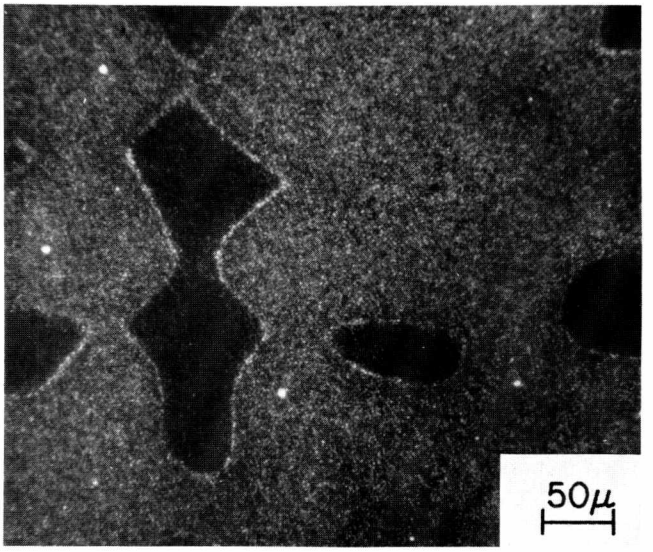

(d)

Fig. 5—Photomicrographs of a specimen annealed at 450°C: (*a*) as-cast; (*b*) 2 hr; (*c*) 3 hr; (*d*) 8 hr.

D at that temperature. Furthermore, if the same relative decrease in $\bar{\rho}\,\bar{c}$ is found at different temperatures, any unknown proportionality constant γ has to be the same. Fig. 8 is then quite strictly a plot of some function $f(\gamma D)$ as a response to $1/T$, where the values of γD are the reciprocals of the transition times (an equivalent choice which gives the same result is obtained from the slope of the log $\bar{\rho}$ vs t plots). The slope of the straight line so obtained is the activation energy for the process when a linear power function is assumed. The slope obtained yields a value of ~ 34 kcal per mole, agreeing quite well with the number found in the literature[11] for the activation energy of copper undergoing bulk diffusion in dilute Al-Cu alloys. Such a result appears to be reasonable evidence that the overall dissolution of nodes is controlled by a bulk diffusion process, which must therefore be the slowest operating mechanism involved.

III) DISCUSSION

The homogenization of a binary alloy apparently can be studied by investigating node dissolution without regard to details of the primary or dendrite structure since a substantive relation between the evolution of nodes and that of a total microsegregation structure has been found. This characterization further supports a view that nodes are prototypes for all the microsegregation pattern which gives a particular insight to the homogenization process. The experimental results behind this conclusion are summarized briefly as follows: Two stages in the evolution of nodes are evident upon annealing, during stage I (early annealing times) dissolution proceeds relatively rapidly, while during stage II (later anneals) the process slows down. The transition from stage I to stage II is particularly sharpened by studying the change of log $\bar{\rho}$ vs time. During stage I, metallographic observations indicate that the *substructure remains morphologically stable* (the cell walls do not disappear while there is second phase in the nodes), while changes are produced in the

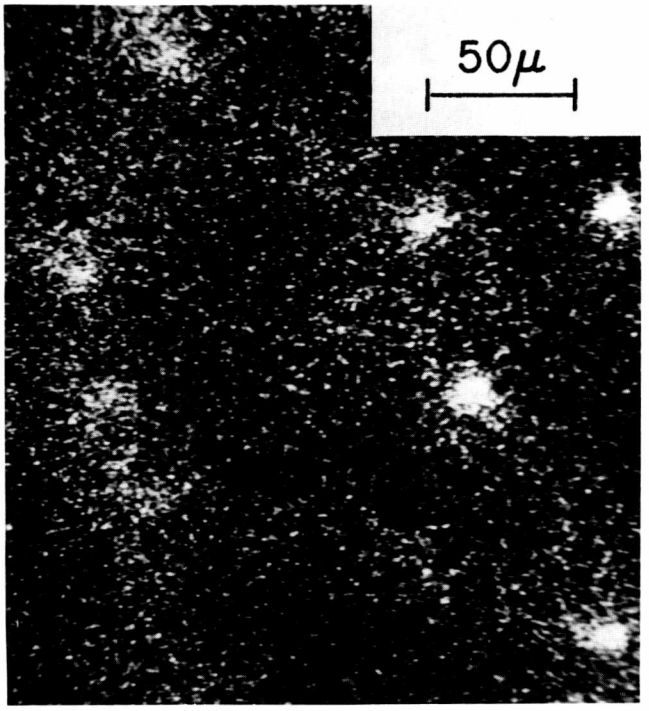

(a)

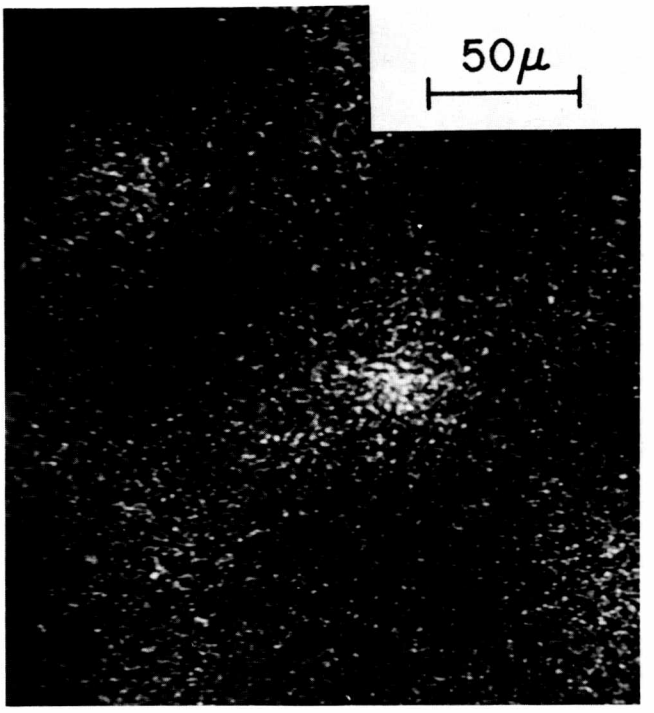

(b)

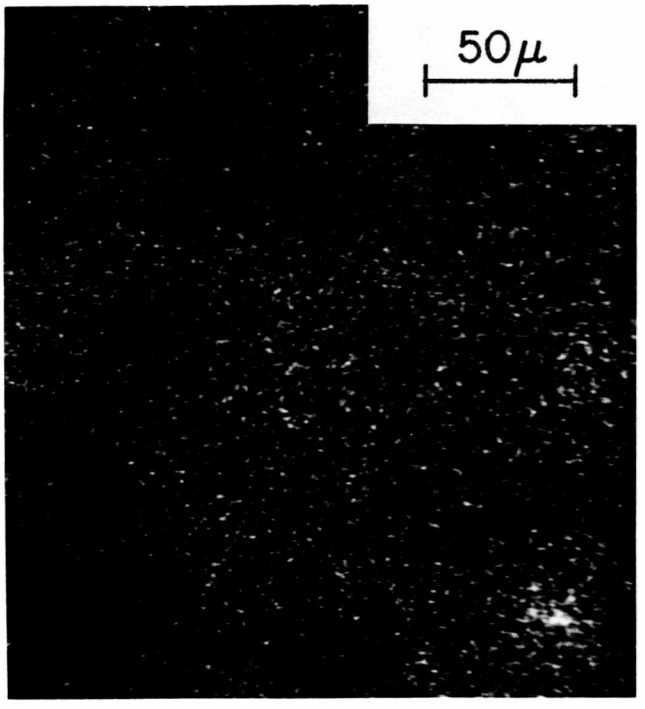

(c)

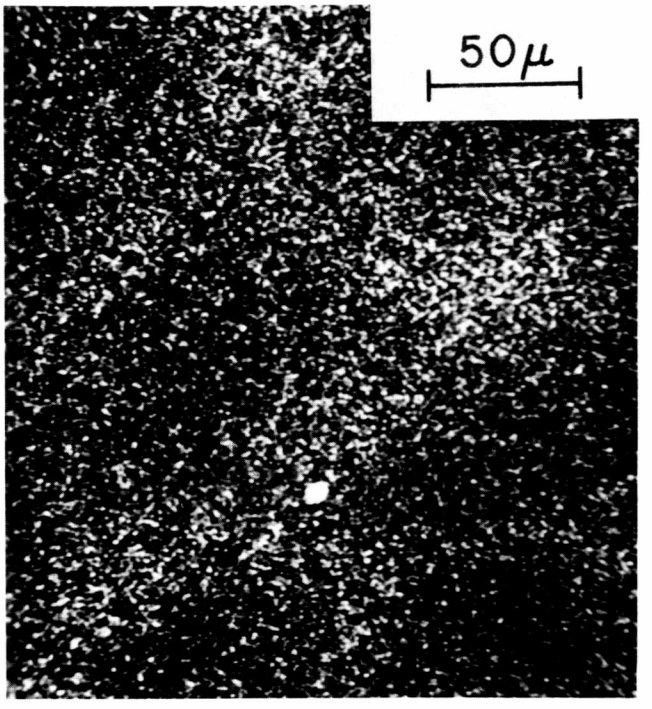

(d)

Fig. 6—X-ray images of a specimen annealed at 513°C: (a) as-cast; (b) 10 min; (c) 15 min; (d) 20 min.

transition to and during stage II with dendritic cells and cell walls slowly disappearing in the final homogenization process.

These observations allow the following particular interpretation. Total morphological stability over an appreciable time (stage I) is most consistent with the idea that during stage I nodes dissolve preferentially along the cell walls. For, the fact that the cell walls of much lower concentration remain evident, while some higher concentration nodes disappear, dictates that they must either be supplied with solute by a dynamic mechanism or concentration stabilized by a static mechanism. There is no reason to suppose any later termination for a static mechanism and yet the walls do disappear later; therefore, a source for solute supply must be considered, and this can only be the nodes. It follows, uniquely in this instance since concentration gradients should favor solute migration towards the matrix, that there must be easier diffusion

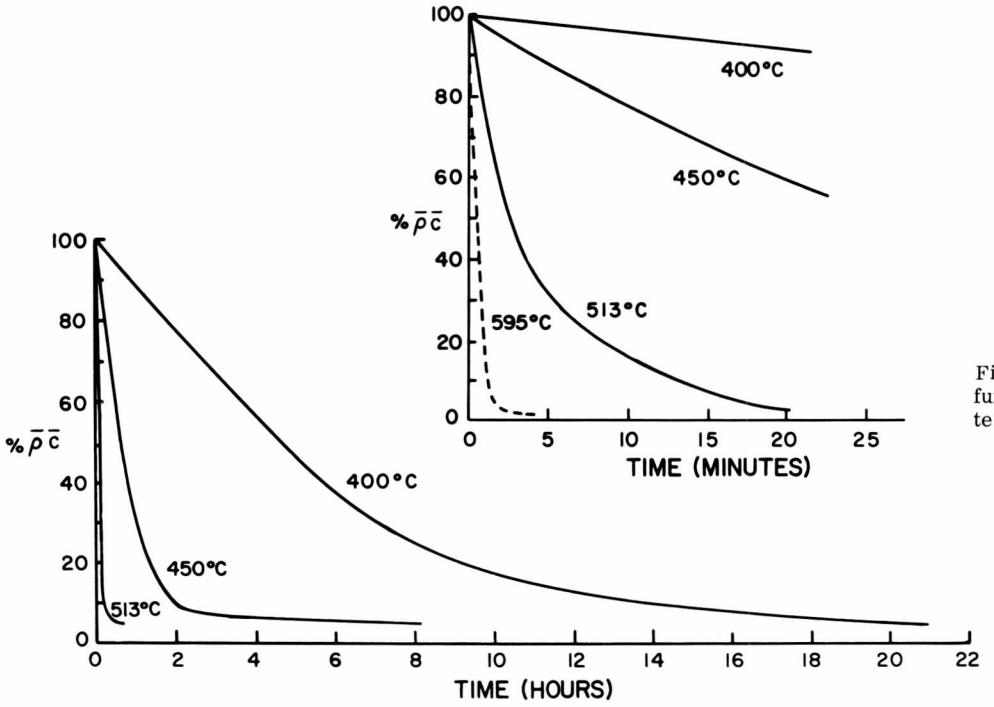

Fig. 7—Normalized values of $\bar{\rho}\bar{c}$ as a function of time for all annealing temperatures.

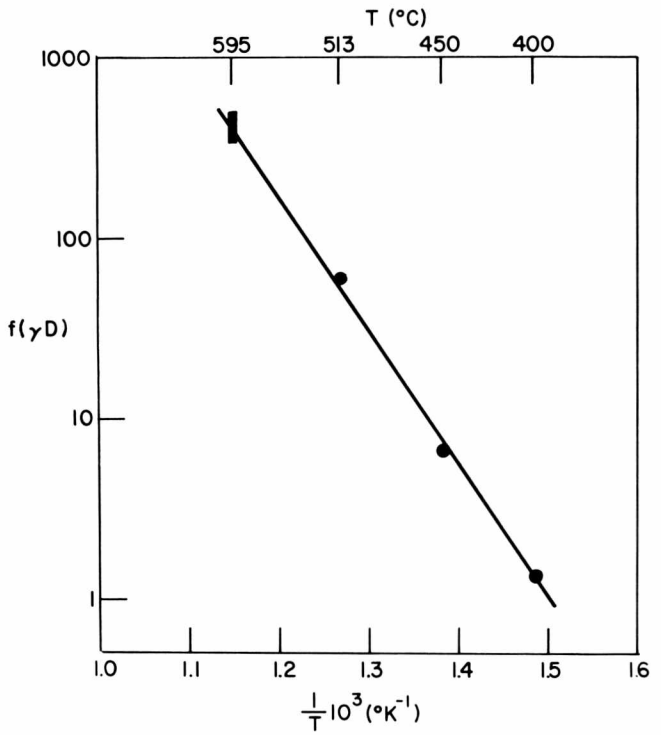

Fig. 8—Reciprocals of the annealing transition times in arbitrary units as a function of $1/T$.

paths around the nodes and along the cell walls. The presence of a high density of dislocations distributed in these boundary regions may provide these paths; the existence of dislocations as related to the solidification substructure is indeed real and well supported by direct observations using electron transmission microscopy.[12] A rough estimate of the density of dislocations along the cell walls can be made for the alloy studied in this work; this gives a reasonable and sufficiently high value of $\sim 5 \times 10^{10}$ cm^{-2}.[13]

In order to explain why the activiation energy for dissolution of nodes obtained during stage I may be the same as that for bulk diffusion of the solute in a dilute alloy, it must be concluded that a collective mechanism operates. That is, we suppose that nodes dissolve preferentially along the cell walls, but acknowledge that their rate of dissolution must eventually (or rather effectively) be controlled by the rate at which solute migrates from the walls into the matrix through a much larger surface. Hence, there must be a more general process which involves the whole substructure and is thus of a collective character. The existence and evolution of nodes in a wide concentration range further but more weakly supports this conclusion. So, in spite of the fact that dissolution proceeds inhomogeneously, the number of nodes and the mean concentration as given by the product $\bar{\rho}\,\bar{c}$ decrease to common values in all the kinetics. The manifest asymmetry in the node concentration distribution maintained through all the anneals, due most probably to the presence of a second phase, is quite consistent with a regulating role attributed to the dislocations.

Morphological instability during stage II can then be easily explained, since the great decrease in the number of nodes and in their solute concentration means that the solute flow from the residual nodes towards the cell walls does not compensate the loss from the walls towards the matrix. This proceeds as a consequence of the existent chemical gradients which drive the homogenization process.

The precise role which dislocations achieve can be evidenced by studies of diverse types. Radiotracer diffusion offers the possibility of observing and measuring the rate of solute migration in the cell walls. Autoradiographic studies made in zinc single crystals with respect to heterodiffusion of nickel[14] clearly revealed the existence and effects of solidification substructure as opposed to diffusion in polygonization walls, which did not appear to provide rapid diffusion paths.

Singh and Flemings[15] and Singh, Bardes, and Flem-

ings[16] have extensively studied the decrease of second phase in as-cast and worked aluminum 7075 (1.35 pct Cu) and Al-4.5 pct Cu and found that although in the worked specimens the dissolution proceeds at a higher rate, the activation energy is always that of bulk diffusion. Several details of their work provide other interesting points; however, we must disagree about the interpretation of dissolution. In their analysis a dependence is placed upon the initial matrix solute distribution and upon the dendrite arm spacing which would correspond for our work to an internode spacing, or some multiple thereof. We have performed a model independent statistical analysis based upon experiments where there is no evidence to support such relations between matrix and second phase (node) concentrations. On the contrary, it seems that local concentration distributions nearby nodes along cell walls should be more controlling than long-range concentrations developing terminally between dendrite arms. In fact, apart from interpretation, some differences in the investigations may reside in the less complex alloy we studied at a much lower copper level of 0.34 wt pct. Theoretical analyses by Heckel and coworkers[17-19] and others[20] suggest local concentration control for this low solute level.

IV) SUMMARY

A main conclusion of this investigation is that homogenization of an alloy is a collective phenomenon. Nodes, of course, do not dissolve independently of the total solidification substructure, but participate in the general process which microsegregation undergoes. Nodes may therefore be used as characteristic measures for microsegregation. Certain conclusions may be derived directly from the experimental observations:

1) The dissolution of nodes proceeds inhomogeneously as revealed by the turning points in the $\bar{c}$ vs t curves.

2) The asymmetry in the node concentration distributions maintained along the whole process is a consequence of the presence of a second phase in a great portion of nodes.

3) Two stages exist in the progress of homogenization and morphological evolution. (This suggests a dislocation regulated process during early anneals due to a high dislocation density present in the cell walls and around the nodes).

4) The activation energy of 34 kcal per mole indicates that the overall homogenization process is volume-diffusion controlled.

ACKNOWLEDGMENTS

The authors are grateful for the encouragement of their colleagues, especially to H. Espejo for his generous and patient assistance during the microprobe examinations and to S. Bermudez for her capable metallography. This research is part of the Programa Multinacional de Metalurgia sponsored by the Organization of American States.

REFERENCES

1. H. Biloni, G. F. Bolling, and G. S. Cole: *Trans. TMS-AIME,* 1966, vol. 236, p. 930.
2. V. V. Damiano and G. S. Tint: *Acta Met.,* 1961, vol. 9, p. 177.
3. K. G. Davis: *Can. Met. Quart.,* 1968, vol. 7, p. 93.
4. S. Siegel: *Non-parametric Statistics for the Behavioral Sciences,* McGraw Hill Book Company, New York, 1956.
5. C. Calvo and H. Biloni: Comisión Nacional de Energía Atómica, Buenos Aires, Argentina, to be published; *Segregación Celular Dendrítica En Aleaciones Al-1 pct Cu,* Publicación Interna Número PMM/C-25.
6. H. Biloni: *Can. J. Phys.,* 1961, vol. 39, p. 1501.
7. H. Biloni, G. F. Bolling, and H. A. Domian: *Trans. TMS-AIME,* 1965, vol. 233, p. 1926.
8. W. J. Dixon and F. J. Massey: *Introduction to Statistical Analysis,* McGraw Hill Book Company, New York, 1957.
9. D. Fainstein: Thesis, Universidad Nacional de Cuyo, Argentina, 1970.
10. H. Espejo: Comisíon Nacional de Energía Atómica, Buenos Aires, Argentina, private communication, 1969.
11. J. B. Murphy: *Acta Met.,* 1961, vol. 9, p. 563.
12. I. Obinata, O. Izumi, D. Oelschlagel, and A. Nagata: *Trans. Japan Inst. Met.,* 1969, vol. 10, p. 107.
13. W. A. Tiller: *J. Appl. Phys.,* 1958, vol. 29, p. 611.
14. J. A. Coll: Rapport de Stage, Centre d'Etudes Nucleaires de Saclay, France, 1966.
15. S. N. Singh and M. C. Flemings: *Trans. TMS-AIME,* 1969, vol. 245, p. 1803.
16. S. N. Singh, B. P. Bardes, and M. C. Flemings: *Met. Trans.,* 1970, vol. 1, p. 1383.
17. R. A. Tanzilli and R. W. Heckel: *Trans. TMS-AIME,* 1968, vol. 242, p. 2313.
18. R. A. Tanzilli and R. W. Heckel: *Trans. TMS-AIME,* 1969, vol. 245, p. 1363.
19. D. L. Baty, R. A. Tanzilli, and R. W. Heckel: *Met. Trans.,* 1970, vol. 1, p. 1651.
20. H. B. Aaron, D. Fainstein, and G. R. Kotler: *J. Appl. Phys.,* 1970, vol. 41, p. 4404.